Segmented Mirror Coarse Phasing with White Light Interferometry: Modeling and Experiment on NGST's Wavefront Control Testbed

Fang Shi[a], David C. Redding[a], Andrew E. Lowman[a], Catherine M. Ohara[a], Laura A. Burns[b], Peter Petrone III[c], Charles W. Bowers[d], and Scott A. Basinger[a]

[a]Jet Propulsion Laboratory, California Institute of Technology, Pasadena, CA 91109
[b]Science Systems and Applications Inc., Lanham, MD 20706
[c]ManTech Systems Engineering Corporation, Greenbelt, MD 20771
[d]Goddard Space Flight Center, NASA, Greenbelt, MD 20771

ABSTRACT

A method of coarse phasing segmented mirrors using white light interferometry (WLI) has been developed for the Next Generation Space Telescope (NGST) wavefront sensing and control. Using the broadband point PSF of the segmented mirrors taken during a segment piston scan, the WLI can accurately detect small residual piston errors. WLI does not rely on extra optics and uses only the final imaging camera. With its high sensitivity to small segment piston error WLI can be used as a complementary phasing algorithm to the dispersed fringe sensor (DFS) for NGST. This paper will present the results from modeling and experiment on the NGST's Wavefront Control Testbed (WCT).

Keywords: Space telescope, segmented mirror, wavefront sensing and control, white light interferometry

1. INTRODUCTION

Segmented mirror coarse phasing is part of the Next Generation Space Telescope (NGST) wavefront sensing and control (WFS&C) process during the early stages of NGST commissioning [1]. It begins after coarse alignment, a process which includes initial capture, tip-tilt alignment, and focusing of each segmented mirror. After coarse alignment, the segmented mirrors are aligned with residual tilt errors less than a fraction of the point spread function (PSF), and focused to within a depth-of-focus (DOF) of each segmented mirror. Although the residual tilts can be handled by the fine phasing, the residual relative pistons (with amplitudes of *~1 DOF*) are still many orders of magnitude too large for the fine phasing algorithm [2]. Coarse phasing with a dispersed fringe sensor (DFS) has been proposed as the segmented mirror coarse phasing technique for the NGST baseline wavefront sensing and control [3, 4] and it has been shown to have adequate dynamic range and accuracy for NGST. However, we have studied another coarse phasing technique based on white light interferometry (WLI). Segmented mirror coarse phasing with WLI uses the features of the white light PSF formed by the segmented mirrors to detect and correct the relative piston between segments. Compared with DFS, coarse phasing with WLI uses only in-focus PSFs and requires no special optics (e.g. grism), and with accurate actuators the WLI can provide piston detection sensitivity better than a few tens of nanometers. However, coarse phasing with WLI requires a large number of in-focus images of a point source as the segment is piston scanned. This limits the WLI's piston detection range to a few microns around the phased position. With its limited range but higher accuracy than DFS, the WLI can be used as next step of coarse phasing after the DFS. There exists other techniques that utilize the features of a broadband PSF to phase the segment mirrors and some are currently being used for the ground-based telescope [5]. The method we proposed, however, gives direct measurement of the segment pistons and requires no special optics. This is significantly beneficial for space telescopes such as NGST.

The WLI piston detection algorithm was developed using realistic optical models. Optical models of various segmented mirror configurations have been established and used to generate white light PSFs. The WLI algorithm has been tested on NGST's Wavefront Control Testbed (WCT). With three segmented mirrors and two deformable mirrors the WCT

provides a flexible testing environment. Various tests have been designed to explore the performance of WLI and the factors that may affect the WLI's performance. The WLI tests on WCT have not only validated the algorithm but also have produced the WLI coarse phasing software as a part of the WCT's Segmented Telescope Control Software (STCS) which enables the user to routinely phase the segmented mirrors on the WCT [6].

In this paper we will introduce the principle of segmented mirror coarse phasing with white light interferometry. We will use the results from both simulations and experiments on WCT to demonstrate the performance of WLI. We will discuss the performance and the characteristics of WLI from the point of view of NGST operation, and finally we will layout the plans for future studies of WLI.

2. WHITE LIGHT INTERFEROMETRY FOR SEGMENTED MIRROR PISTON DETECTION

The wavefront of a segmented-mirror telescope is the combination of the wavefront of each individual segment, and the broadband PSF is the result of the white light interferences of the segments. At the image plane, the phases of the electromagnetic field from two segments which have a relative wavefront piston δL is

$$\begin{aligned} \phi_1 &\sim e^{ikL} \cdot e^{-i\omega t}, \\ \phi_2 &\sim e^{ik(L+\delta L)} \cdot e^{-i\omega t} \end{aligned} \tag{1}$$

where $k = 2\pi/\lambda$ is the wave number and L is the common path length. The time-averaged monochromatic intensity at the image plane can be written as

$$I(\theta) = 2I_{seg}(\theta) \cdot \left[1 + \gamma \cos\left(\frac{2\pi}{\lambda} (d\theta + \delta L) \right) \right] \tag{2}$$

where θ is the angular image plane coordinate, d is the base-line distance between the two segments, and $I_{seg}(\theta)$ is the PSF of one mirror segment. The visibility constant γ is determined by factors such as the source size, the segment mirror figure error, or, if present, other segments to contribute to the total intensity of $I(\theta)$. For the case of two ideal segments with equal area illuminated by a point source, the visibility is $\gamma = 1$. For a circular segmented mirror with diameter D, the single segment PSF $I_{seg}(\theta)$ is simply

$$I_{seg}(\theta) = A \cdot \left[\frac{2J_1(\pi\theta D/\lambda)}{\pi\theta D/\lambda} \right]^2 D^2 \tag{3}$$

Eq. 2 shows that the relative wavefront piston between the segmented mirrors will form an intensity modulation within the envelope of the PSF formed by the segment $I_{seg}(\theta)$. The intensity modulation depends on the wavefront piston as well as the wavelength, forming a dark band I_{min} and bright band I_{max} when the conditions are as follows:

$$\begin{aligned} I_{\min} &\Leftrightarrow \frac{2\pi}{\lambda}(d\theta + \delta L) = (2n-1)\pi \\ I_{\max} &\Leftrightarrow \frac{2\pi}{\lambda}(d\theta + \delta L) = 2n\pi \end{aligned} \tag{4}$$

where $n = 1, 2, \ldots$is an integer. Therefore, for monochromatic light, as the piston δL increases the modulation within the PSF will repeat. If we try to use the modulation relations defined in Eq. 4 to detect the segment relative piston δL we would encounter the ambiguity problem because we can not determine the integer n in Eq. 4. However, the ambiguity problem can be solved by using a white light source. When integrate the Eq. 3 over the wavelength of a white light source with wavelength bandwidth of $\Delta\lambda$ centered at λ_0, the center intensity $I(\theta = 0)$ will have the form of [7],

$$I(0) = 2I_{seg}(0)\cdot\Delta\lambda\left[1+\gamma\left(\frac{\sin\left(\frac{\pi\Delta\lambda}{\lambda_0^{\,2}}\delta L\right)}{\frac{\pi\Delta\lambda}{\lambda_0^{\,2}}\delta L}\right)\cos\left(\frac{2\pi}{\lambda}\delta L\right)\right] \tag{5}$$

The *sinc* function in Eq. 5 shows that for a broadband source, the visibility of the modulation due to the piston depends on the spectral bandwidth $\Delta\lambda$ as well as the piston error δL. In addition, the intensity modulations within the PSF are most visible when the piston error δL is smaller than the coherence length defined as $\lambda_0^2/\Delta\lambda$. Segmented mirror coarse phasing with white light interferometry uses this intensity modulation within the broadband PSF to sense the relative piston between the segments.

WLI signal is formed from the center pixel intensity of the image. Figure 1 shows a modeled WCT WLI signal versus segment piston position. While one segment's piston is scanned from $\delta L = -5\ \mu m$ to $+5\ \mu m$ with a step size of $0.01\ \mu m$, a broadband PSF image is generated for each piston position and the center pixel intensity is extracted to be the WLI signal. The under-sampled image in WCT has lowered the visibility but as shown in the figure the modulation is still quite strong. Two wavelength bandwidths are simulated here to reflect the testbed source setup, one with FWHM bandwidth of *220 nm* and the other with *300 nm*. Figure 2 shows some sample PSF images of the piston scan around the segments being phased. The piston values selected are the same for both filter bandwidths. The plot shows that when the relative piston is zero the segments are phased and wavefront from all the wavelengths are coherently added, therefore creates the maximum peak of WLI signal. Compared to the plots in Figure 1 and PSF images in Figure 2 we can see the effect of wavelength bandwidth and coherence length on the WLI signal: a broader bandwidth narrows the piston range in which the PSF modulation is visible.

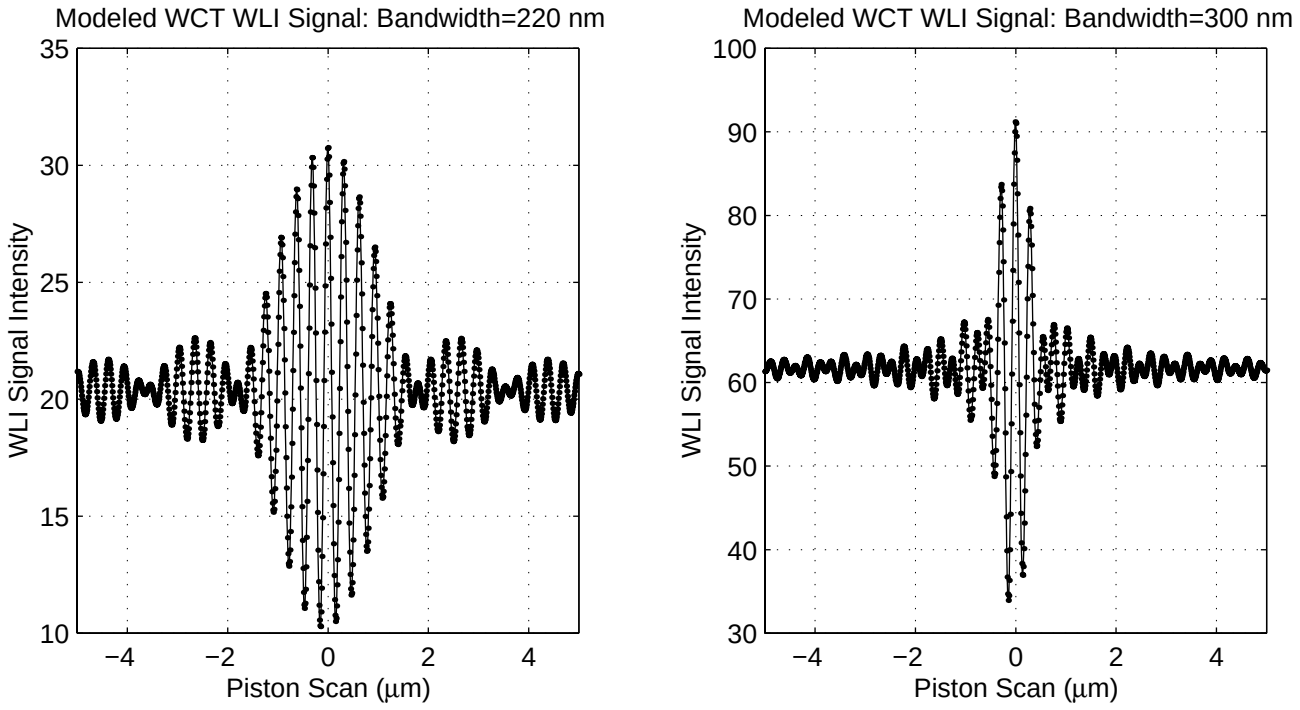

Figure 1. Modeled WCT broadband PSF center pixel intensity versus segment #3 piston position. Segment #2 is used as the reference segment. *Left*: WLI signal with a *220 nm* bandwidth filter. *Right*: WLI signal with a *300 nm* bandwidth filter. Both wavelength filters are centered at *633 nm* and the model assumes a flat spectrum.

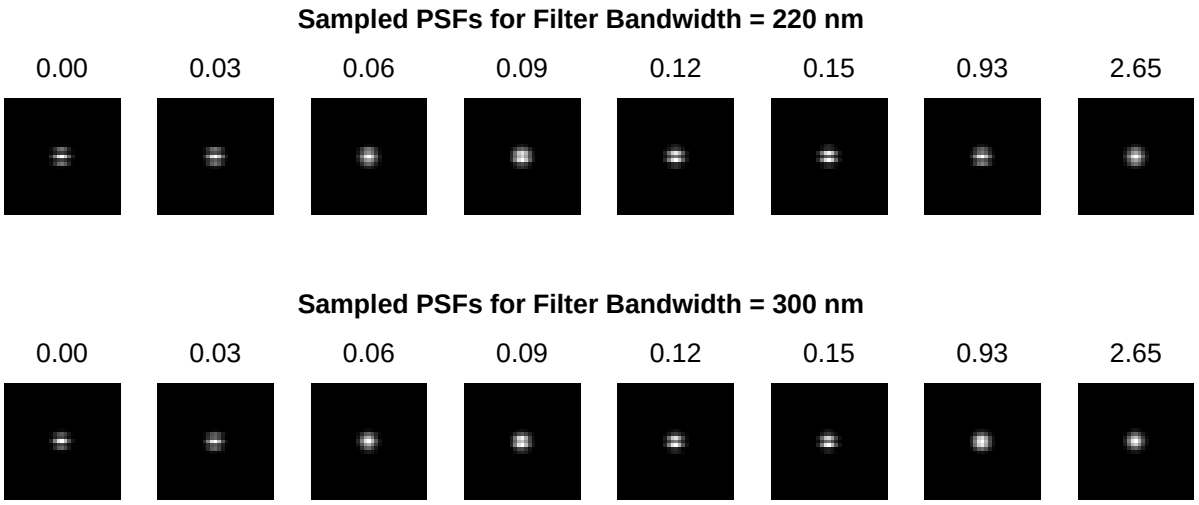

Figure 2. Selected sample PSF images from the WLI piston scan. The piston values are shown above each image in units of microns. *Top row*: WLI PSFs with *220 nm* bandwidth. *Bottom row*: WLI PSFs with *300 nm* bandwidth. When piston changes from 0 to 0.15 μm the center pixel intensity goes from the maximum to the first minimum. For intermediate pistons such 0.93 μm WLI modulations is visible only for the narrower filter (220 nm), and at large pistons modulation from white light interferometry is totally washed out, forming a PSF of the size of a single segment.

The process of using WLI to sense and correct the relative segment piston is as follows: First, a broadband point source is required. As indicated in Eq. 2, a extended source may lower the visibility of the modulation. Second, the filter bandwidth should be selected according to the expected piston error. The coherence length of the filter should be larger than the piston to be detected. When the segments are phased with a DFS, which can reduce the piston error to within *0.1 μm*, a broader bandwidth filter (*> 220 nm*) can be used for taking WLI signal. The piston scanning range is determined according to the selected filter – a narrower filter provides a larger the piston scan range. Without knowledge of the piston error the piston scanning is always centered from the current segment piston position. Third, scan the piston of the segment to be phased with a small step size, taking an image at each piston step and recording the actuator positions. The minimal piston scanning step size, which affects the WLI sensitivity and final accuracy, is determined by the segment aperture size and the base-line distance between the two segments. Fourth, extract the center pixel intensity from each piston scanning PSF image. For the data from WCT, which currently does not have a closed loop fast-steering mirror, a centroid calculation is required to determine the center pixel. The relation of the PSF center pixel intensity versus piston position is the WLI signal for that segment. Finally, the piston is determined from the WLI signal by locating the position at which the signal is at a maximum. However, random fluctuations in WLI signal caused by detector noise and environmental effects will make piston detection unreliable if the piston is detected directly using the peak intensity of WLI (Figure 4). A more reliable method is to use the maximum of the cross correlation between the measured WLI signal and the ideal WLI template generated from modeling to detect the piston. Because the cross correlation uses all the points in the WLI signal it significantly reduces the influence of the noise fluctuation in the signal, thus resulting in a more reliable piston detection. Figure 3 shows the results from a WCT simulation in which segment #3 had an initial piston error of *–1.0 μm*. Random noise equal to *10%* of the peak intensity of the PSFs was added to the WLI signal, producing a very noisy WLI signal. However, the correlated signal generated by cross correlating the noisy WLI signal with the theoretical template shows a very clean peak, which in turn provides a more robust and accurate piston detection. For the WLI signal shown in Figure 3, using the peak intensity of WLI signal would have yielded an incorrect piston of *–1.04 μm*, while using the correlation method produced the correct the result of *–1.00 μm*. This simulation demonstrates the effectiveness of detecting segment piston with the correlation method.

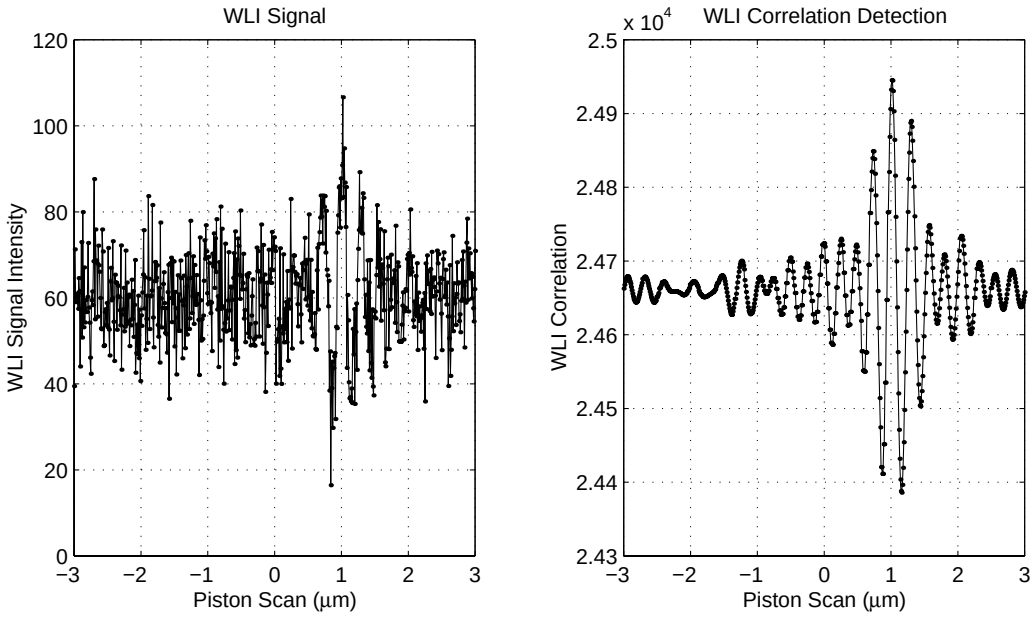

Figure 3. *Left*: Modeled WCT WLI signal with segment #3 pistoned by *–1.0 μm* and segment #2 used as the reference segment. The 300 nm filter is used. A significant amount of random noise was added to the WLI piston scan images to deliberately produce a very noisy WLI signal. *Right*: The cross correlation using the ideal template to detect the segment piston.

Once the segment piston has been measured by WLI, the control software can drive the segment's actuators to remove the piston error and therefore phase the two segments. The phased segments can then be used as the reference segment, and the process can be repeats to phase the remaining segments. As more segments are phased together, or "built up" to form the reference, the difference between the aperture area of the reference segment and the area of the segment being phased will increase. This may reduce the contrast of the modulation within the PSF (the γ in Eq. 2) and therefore reduce the visibility of WLI signal. However, for a system with a large number of segmented mirrors, the segments can be divided into groups and PSF centers of these groups can be separated so that every piston scanning image will contain several PSFs, one for each group. In this fashion, the WLI process can be done simultaneously for each group. After phasing all the segments within each group, each phased group can be treated as a single segment and WLI will then phase the "grouped segments" together to form a completely phased aperture. The segment grouping will not only increase the WLI efficiency but also avoid the poor WLI signal visibility due to segment build-up.

3. WLI EXPERIMENTS ON WAVEFRONT CONTROL TESTBED

The NGST's WCT is a modular system which consists of (1) the Source Module which provides a broadband point source with a set of narrow and broad band filters, (2) the Simulator Module which can generate high-order aberrations using a 69-actuator deformable mirror (SMDM) and a wavefront piston using a set of transmissive phase plates, or contains three segmented mirrors that each can be accurately tilted and pistoned, (3) the Aft-Optics Module which contains a one-to-one imaging system, a 349-actuator deformable mirror (AODM) for wavefront correction, a fast steering mirror, a flip-in grism, and a CCD camera on a translation stage. The segmented mirrors in the WCT consist of three one-inch diameter spherical mirrors which are conjugate to the system aperture defined by the AODM. Each segmented mirror is driven by a PZT platform with 3 piezoelectric actuators which provide nanometer level control over a 12 μm range. Compared to the full aperture of DM the three segmented mirror form a sparse aperture with the segmented mirrors cover only about 30% of total aperture area formed by DM. The WCT is physically located at Goddard Space Flight Center and most of the experiments are run via the Internet from JPL by the WCT's Segmented

Telescope Control Software (STCS) [6]. More detailed information of about the WCT hardware setup and capability can be found in references [8, 9, 11, 12].

A graphical user interface (GUI) has been developed for WCT WLI which allows the user to select the reference segment(s), the segment to be phased, the wavelength filter, and to specify the WLI piston scanning range and step size. To limit the number of images needed, a WLI experiment on WCT is usually started after running WCT coarse alignment and coarse phasing with a DFS. Due to the testbed environment perturbations such as the lab seeing, testbed jittering and drifting, the PSF images taken during the piston scan are blurred and the PSF centroid positions move around by as much as a pixel. To extract the WLI signals from the center pixel of the PSFs, the centroid of the PSF is calculated and the WLI signal is interpolated at the center position of each PSF. The fact that the WCT's PSF is under-sampled causes even more fluctuation of the WLI signal. As mentioned in Section 2, using the entire WLI signal to cross correlate with the template significantly reduces the influence of the WLI signal fluctuations. Figure 4 demonstrates the close loop performance of WLI on the WCT. The plots show the broadband PSFs and WLI signals before and after the piston correction. The final residual piston is related to the piston scan step size and the WLI shows that there is *20 nm* residual piston which is equal the piston step size in the experiment. An independent wavefront sensing using the In-focus PSF Optimizer (IPO) [10] was performed after the WLI correction and verified that the residual piston on the segment was *13 nm*.

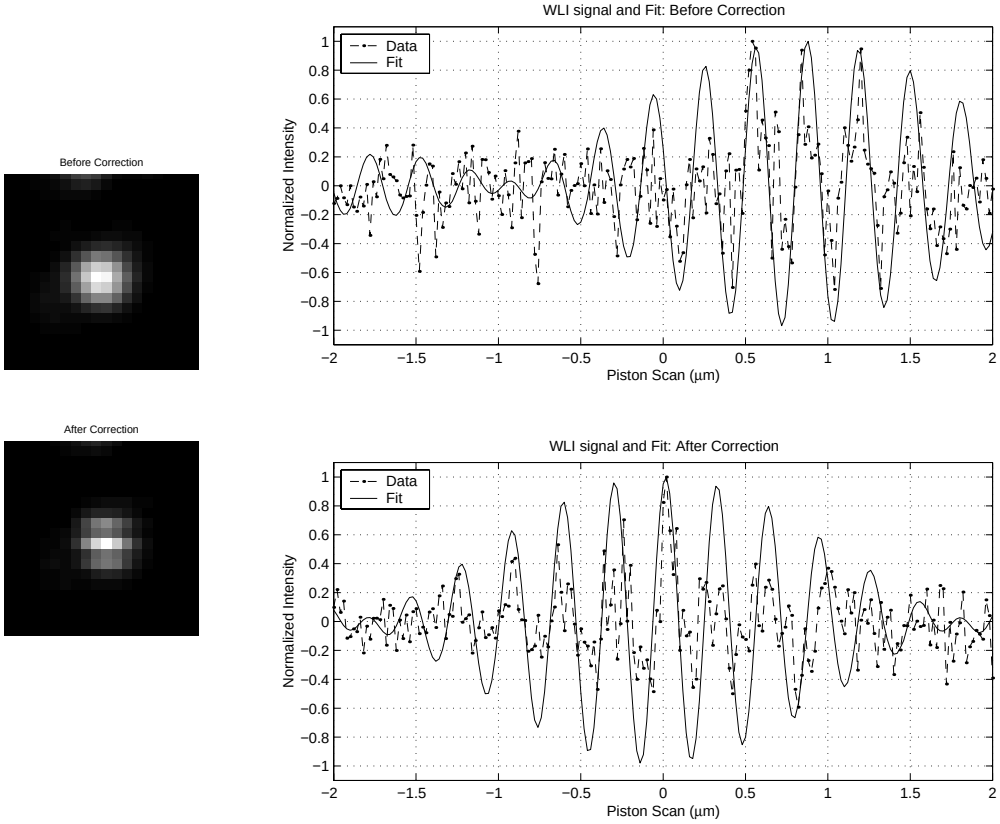

Figure 4. WLI demonstration on WCT: segment #2 is the reference and segment #3 is being phased. *Upper left*: broadband PSF before segments are phased. The unphased PSF has a size and shape equivalent to that of a single segment. *Upper right*: WLI signal and WLI piston solution fit before correction. The WLI has detected the segment #3 piston is *–0.88 μm*. *Lower left*: broadband PSF after being phased. *Lower right*: WLI signal and WLI piston solution fit after correction. The WLI has detected a residual piston of *20 nm*. The *220 nm* bandwidth filter was used for this experiment.

The effect of segment build-up was also studied on WCT. In the experiment, a WLI signal was first taken with only one reference segment in. Then a WLI signal was taken with two phased segments as the reference segment. The WLI signals as well as PSFs at which the WLI signals are at maximal are shown in Figure 5. The WLI signals and the PSFs

have shown that there are two competing effects from the segment building up: on one hand, as more segments are included in as the reference segments the mean WLI signal level increases from the increase of the total collecting aperture area. This will lower the WLI signal visibility and increase the photon noise hence lower the signal to noise ratio (SNR) of WLI. On the other hand, however, as more segments being phased the peak intensity oscillation of WLI signal will increase because the PSF size is smaller due to the total area increase. This will improve the WLI signal's SNR. The end result of the segment building up will depend on the image sampling, aperture sparseness, and segment base line distance. Simulation has shown that for a system with large number of segments the adverse effect of segments build-up is dominant and phasing segment by dividing the segments into groups will be a suitable approach.

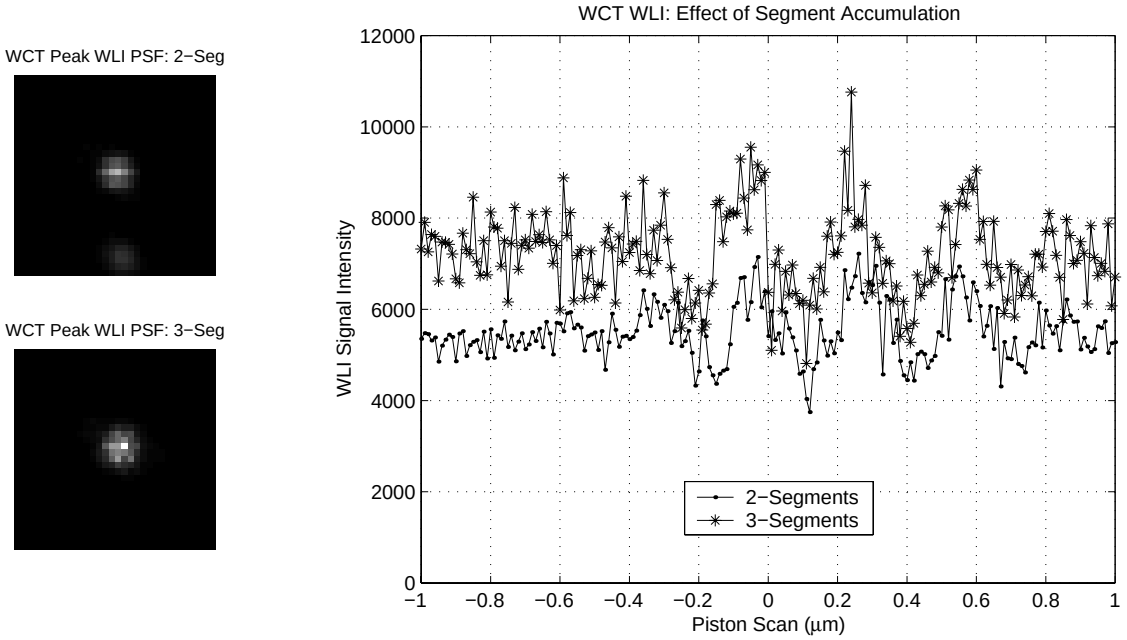

Figure 5. WLI experiment on the effect of segment build-up. *Left panel*: PSFs when WLI signal intensity is at maximum. The top image is from 2 segments and the bottom is that of all 3 segments. *Right panel*: Comparison of WLI signals with one and two segments used as reference. The WLI signal from all 3 segments is higher due to the larger collecting area.

4. CONCLUSIONS AND FUTURE WORK

Segmented mirror coarse phasing with white light interferometry is a different approach compared with the dispersed fringe sensor. WLI provides finer piston sensitivity (*10 ~ 20 nm*) but requires more images than DFS. Because WLI uses the piston scan as its signal, the WLI segment piston sensing and correcting also depends on the linearity and accuracy of the segmented mirror actuators. In the NGST wavefront sensing and control, the process of coarse phasing with a DFS has already provided enough dynamic range and accuracy to handle the segment piston between the coarse alignment and fine phasing [4]. However, since it requires no other special optics other than a broadband filter the WLI can be used as an alternate segment piston sensing and control method for NGST.

Experiments on WCT have validated the modeling results and demonstrated the closed loop performance of WLI on the testbed. Coarse phasing with WLI has been used in the routine operation of the testbed and the WLI control software has been integrated with the testbed's STCS.

More modeling studies and WCT experiments will follow. These include tests to explore the robustness under adverse conditions such as the segmented mirror surface aberrations and radius mismatch. Modeling and experiments will also be carried out to define the best strategy of choosing the filter bandwidth, piston scanning range, and piston step size to

optimize the WLI dynamic range and final accuracy. The WCT is evolving and will provide us with more test capabilities and prepare the WLI algorithm close to the real NGST hardware characteristics.

5. ACKNOWLEDGEMENTS

The work reported here is the result of effort from all the members in the NGST wavefront sensing and control team both at Jet Propulsion Laboratory and Goddard Space Flight Center. This work was performed at the Jet Propulsion Laboratory, California Institute of Technology, under contract with the National Aeronautics and Space Administration.

6. REFERENCES

[1] D. Redding, S. Basinger, C. Bowers, R. Burg, L. Burns, D. Cohen, B. Dean, J. Green, A. Lowman, C. Ohara, and F. Shi, "Next Generation Space Telescope wavefront sensing and control," SPIE paper **4850**-49, Waikoloa, Hawaii (2002).

[2] D. Redding, S. Basinger, C. Bowers, L. Burns, D. Cohen, B. Dean, P. Dumont, J. Green, A. Lowman, C. Ohara, and F. Shi, "Image-based wavefront sensing and control experiment," SPIE paper **4850**-62, Waikoloa, Hawaii (2002).

[3] F. Shi, D. Redding, C. Bowers, A. Lowman, S. Basinger, T. Norton, P. Petrone, P. Davila, M. Wilson, and R. Boucarut, "DCATT dispersed fringe sensor: modeling and experimenting with the transmissive phase plates," Proc. SPIE **4013**, 757 – 762, Munich, Germany (2000).

[4] F. Shi, D. Redding, A. Lowman, C. Bowers, L. Burns, P. Petrone, C. Ohara, and S. Basinger, "Segmented mirror coarse phasing with a dispersed fringe sensor: experiment on NGST's Wavefront Control Testbed," SPIE paper **4850**-51, Waikoloa, Hawaii (2002).

[5] G. A. Chanan, M. Troy, F. G. Dekens, S. Michaels, J. Nelson, T. Mast, and D. Kirkman, "Phasing the mirror segments of the Keck Telescopes: the broadband phasing algorithm," *Applied Optics*, **101**, pp. 140-155, Jan. 1998.

[6] S. Basinger, D. Redding, F. Shi, D. Cohen, J. Green, C. Ohara, A. Lowman, L. Burns, "Wavefront sensing and control software for a segmented space telescope," SPIE paper **4850**-56, Waikoloa, Hawaii (2002).

[7] A. F. Boden, "Elementary theory of interferometry," *Principles of long baseline stellar interferometry*, P. R. Lawson, ed., 9 – 27, 1999.

[8] A. Lowman, F. Shi, D. Redding, S. Basinger, C. Bowers, and P. Davila, "Telescope simulator for the DCATT testbed," Proc. SPIE **4013**, 954 – 961, Munich, Germany (2000).

[9] P. Petrone, S. Basinger, C. Bowers, D. Cohen, L. Burns, A. Chu, P. Davila, P. Dogota, B. Dean, J. Green, K. Ha, W. Hayden, D. Lindler, A. Lowman, C. Ohara, D. Redding, F. Shi, M. Wilson, and B. Zukowski, "Optical design and performance of the NGST wavefront control testbed," SPIE paper **4850**-55, Waikoloa, Hawaii (2002).

[10] C. Ohara, D. Redding, F. Shi, and J. Green, "PSF monitoring and in-focus wavefront control for NGST," SPIE paper **4850**-64, Waikoloa, Hawaii (2002).

[11] NGST's WCT public web site: http://www.ngst.nasa.gov/Hardware/text/WCT.html

[12] L. Burns, S. Basinger, T. Beck, J. Deering, D. Tonnu, D. Lindler, A. Lowman, R. Morris, C. Ohara, P. Petrone, D. Redding, J. Schott, S. Stoner, and L Wheeler, "Wavefront Control Testbed integrated software system," SPIE paper **4850**-58, Waikoloa, Hawaii (2002).